Author Manuscript

Title: From Selection to Instruction and Back — Competing Conformational Selection and Induced Fit Pathways in Abiotic Hosts

Authors: Jovica D Badjic, Prof.; Radoslav Z Pavlović; Remy F Lalisse; Alexandar L Hansen; Christopher A Waudby; Lei Zhiquan; Murat Guney; Xiuze Wang; Christopher M Hadad

To be cited as: 10.1002/anie.202107091

Link to VoR: https://doi.org/10.1002/anie.202107091

From Selection to Instruction and Back — Competing Conformational Selection and Induced Fit Pathways in Abiotic Hosts

Radoslav Z. Pavlović,[a] Remy F. Lalisse,[a] Alexandar L. Hansen,[b] Christopher A. Waudby,[c] Zhiquan Lei,[a] Murat Güney,[d] Xiuze Wang,[a] Christopher M. Hadad,[a] Jovica D. Badjić[a]*

[a] R.Z. Pavlović, R. F. Lallise, Dr. Z. Lei, X. Wang, Prof. C. M. Hadad and Prof. J. D. Badjić
Department of Chemistry & Biochemistry
The Ohio State University
100 West 18th Avenue, Columbus, Ohio 43210, United States
E-mail: badjic.1@osu.edu
[b] Dr. A. L. Hansen
Campus Chemical Instrument Center
The Ohio State University
100 West 18th Avenue, Columbus, Ohio 43210, United States
[c] Dr. C. A. Waudby
Institute of Structural and Molecular Biology
University College London
WC1E 6BT United Kingdom
[d] Prof. M. Güney
Agri Ibrahim Çeçen University,
Department of Chemistry
04100, Agri, Turkey

Supporting information for this article is given via a link at the end of the document.

Abstract: Two limiting cases of molecular recognition, induced fit (IF) and conformational selection (CS), play a central role in allosteric regulation of natural systems. The IF paradigm states that a substrate "instructs" the host to change its shape after complexation, while CS asserts that a guest "selects" the optimal fit from an ensemble of preexisting host conformations. With no studies that quantitatively address the interplay of two limiting pathways in abiotic systems, we herein and for the first time describe the way by which twisted capsule ***M*–1,** encompassing two conformers ***M*–1**(+) and ***M*–1**(–), traps CX_4 (X = Cl, Br) to give CX_4⊂***M*–1**(+) and CX_4⊂***M*–1**(–), with all four states being in thermal equilibrium. With the assistance of 2D EXSY, we found that CBr_4 would, at its lower concentrations, bind ***M*–1** via ***M*-1**(+)→***M*–1**(–)→CBr_4⊂***M*–1**(–) pathway corresponding to conformational selection. Nudged elastic band (NEB) coupled with density functional theory (DFT) computations revealed the mechanism of ***M*-1**(–)/***M*–1**(+) interconversion from which we deduced that the reduced rate for CX_4⊂***M*–1**(–) converting into CX_4⊂***M*–1**(+) resulted from favorable C—H···Cl/Br—C host-guest contacts stabilizing the corresponding ground state. For ***M*–1** complexing CCl_4 though, we used data from 2D EXSY measurements and 1D NMR lineshape analysis to characterize the dynamics of every elementary step in the four-state equilibrium. Subsequently, the contribution of IF and CS was determined using flux analysis wherein the mass transport (i.e. flux) through each particular pathway was quantified. Importantly, we found that lower CCl_4 concentrations would favor CS while the IF pathway prevailed at higher proportions of the guest. Since CS and IF are not mutually exclusive, we reason that our work sets the stage for characterizing the dynamics of a wide range of already existing hosts to broaden our fundamental understanding of their action. The objective is to master the way by which encapsulation takes place for designing novel and allosteric sequestering agents, catalysts and chemosensors akin to those found in nature.

Introduction

Metabolites, neurotransmitters, hormones and pharmaceuticals aim for regulatory sites within receptor proteins to direct physiological processes via propagating conformational changes.[1] A fundamental understanding of such allosteric events[2] has been of a great interest for designing more effective drugs targeting enzyme catalysis, cell metabolism, gene transcription and signal transduction.[3] So far, two limiting cases of allostery play a central role in biological systems described by induced fit (Koshland-Nemethy-Filmer model, top in Figure 1)[4] and conformational selection (Monod-Wyman-Changeux, bottom in Figure 1)[5] formalisms. Induced fit (IF) paradigm[6] states that upon a ligand binding a set of "instruction" is provided to induce a change in the conformation (Figure 1). On the other hand, conformational selection (CS) asserts that a protein exists in a discrete set of conformations of which only the "optimal" one binds to its ligand to become stabilized and increase in concentration (Figure 1).[7] With the advancement in experimental and theoretical means for probing the structure and dynamics of complex biological molecules, the ongoing debate about the occurrence of CS vs. IF is, under examined experimental conditions, settling in favor of the former one.[3] In this regard, recent studies have shown that two limiting

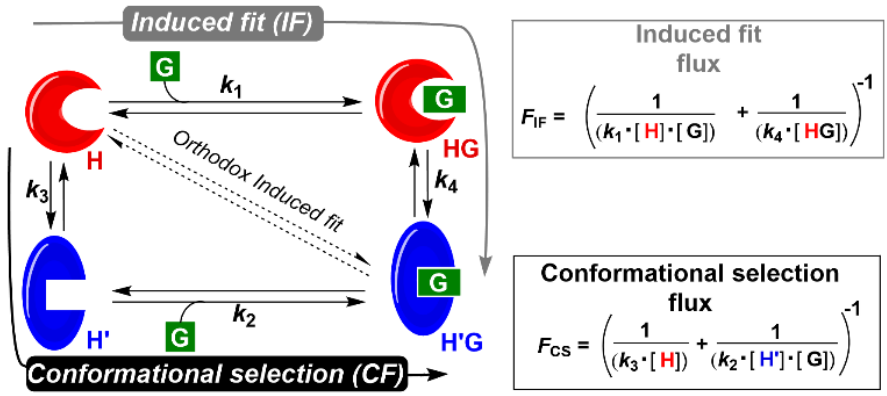

Figure 1. (Left) The Monod-Wyman-Changeux (MWC) scheme describing induced fit (top) and conformational selection (bottom) routes by which two conformers of host H (more stable) and H' (less stable) complex guest G. Diagonal conversion depicts a case of the orthodox induced fit (i.e. Koshland-Nemethy-Filmer) paradigm. (Right) The mass transport or flux (F) of induced fit (F_{IF}) and conformational selection (F_{CS}) pathways can be calculated for a system under equilibrium using rate coefficients and equilibrium concentrations of host and guest.

mechanisms are not mutually exclusive and can take place concurrently.[8] For a large variety of abiotic hosts,[2b, 9] only a handful of studies[10] address the two mechanistic paradigms. The Raymond-Bergman-Toste[11] and Jiang[12] teams have recently measured kinetics by which an encapsulation equilibrium is established to find that CS dominates entrapments promoted by self-assembled metallacages and naphtotube macrocycles with guest molecules in excess. On the other hand, the equilibria as well as concentrations of participating species. Next, the relative flux (i.e. mass transport rate) through the competing CS and IF pathways is calculated using equations in Figure 1 to disclose the proportion of the two mechanistic alternatives under desired conditions.[8a] With abiotic hosts, whose structure and dynamic characteristics are often more straightforward to elucidate by NMR spectroscopy than their biological counterparts, it is surprising that there are not yet any detailed studies about the interplay of the two pathways. The results of such work will not only improve the design of allosteric supramolecular sequesters,[14] delivery agents[15] or catalysts[16] operating under a particular set of conditions, but may also shine more light on the mechanisms by which complex biological molecules relay chemical signals.

Recently, we reported[17] about twisted capsule ***M*–1** (Figure 2A) binding haloalkanes CBr_4 and CCl_4. In particular, CX_4 (X=Cl, Br) stabilized the ***M*–1**(–) conformer (Figure 2B) using three C—H···X—C host-guest interactions depicted for CX_4⊂***M*–1**(–) in Figure 2C; note that prefix ***M*** is used to depict the anticlockwise sense of helical twist of the aromatic arms from the cup (when viewed from the bottom, Figure 2A), while

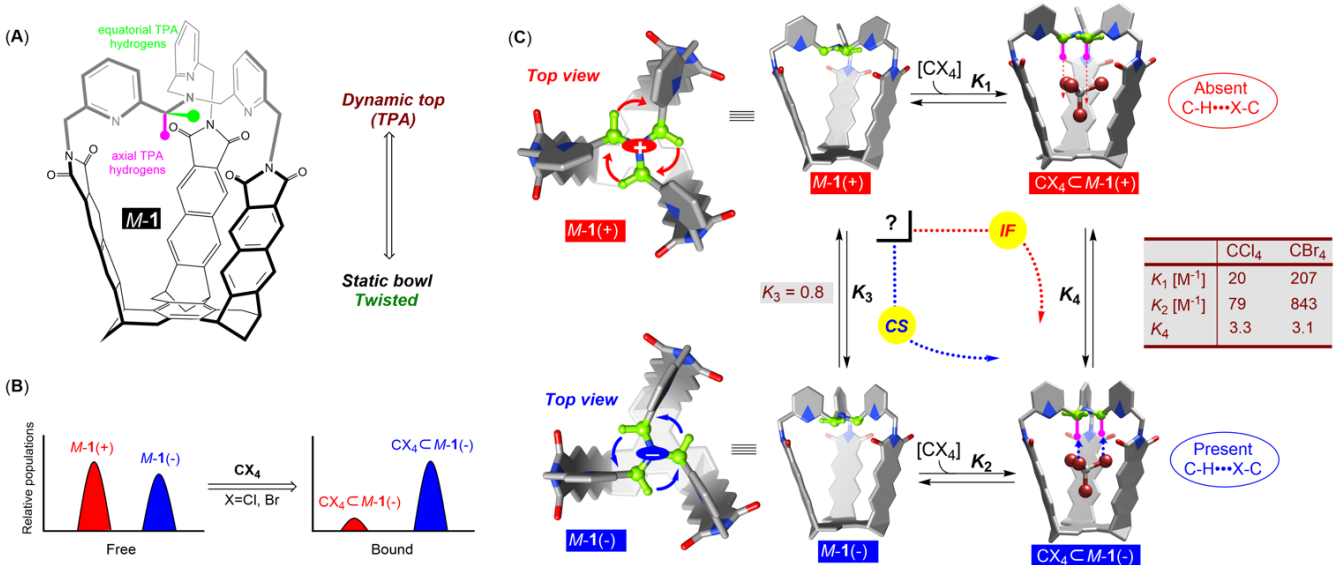

Figure 2. (A) Structure of capsule ***M*–1** comprising a twisted cup (anticlockwise or ***M***, when viewed from the bottom) and conformationally flexible TPA group on top. (B) A schematic depiction of guest-responsive behaviour of ***M*-1**, where guest binding alters the populations of the two conformations found in equilibrium. (C) Energy-minimized structures of ***M*–1**(+), ***M*–1**(–), CBr_4⊂***M*–1**(+) and CBr_4⊂***M*–1**(–) with equilibrium constants K_1–K_4 (with c.a. 5% uncertainty from NMR signal integration) obtained from ^{1}H NMR spectroscopy at –95 °C;[16] note that aromatic *tris*-(2-pyridylmethyl)amine (TPA) lid on top of ***M*–1** assumes two positions about its C_3 axis, with top TPA N-C-**H** (green) aiming either clockwise ***M*–1**(+) or anticlockwise ***M*–1**(–) when viewed from top.

the Hiraoka team[13] suggested that IF took place through expansion and contraction of self-assembled nanocubes in the encapsulation of guests. Importantly, it has been shown that at different equilibrium concentrations of participating species the two limiting mechanisms may, in biological systems, occur either concurrently or one can outcompete another.[8a] In other words, to develop a full mechanistic understanding of the system of interest, one has to determine rate coefficients characterizing the suffix (–) corresponds to the anticlockwise sense of rotation of three methylene C–H groups when viewed from the top (green in Figure 2C). These interactions were absent in the less stable CX_4⊂***M*–1**(+) (Figure 2C). After the formation of CBr_4⊂***M*–1**(+) and CBr_4⊂***M*–1**(–), low temperature ^{1}H NMR spectra showed all four species in equilibrium at –95 °C (K_1–K_4, Figure 2C).[17] Accordingly, we used the Monod-Wyman-Changeux scheme (MWC, Figure 2C) to outline the exchange

among the four states. Since multiple pathways could join these states, we wondered if any of them would dominate the process. That is to say, how does CS and IF direct the encapsulation in twisted capsules (Figure 1) under different experimental conditions?[8] With the system being suitable to study by both computational methods[17] and NMR spectroscopy,[18] we set out to probe its kinetics. The results from quantitative 2D EXSY measurements,[19] lineshape analysis and nudged elastic band (NEB)[20] coupled with density functional theory (DFT) suggest CS being the principle way by which capsule ***M*–1** trap/release halocarbons at lower concentrations. At higher concentration of haloalkanes, a switch in the mechanism takes place to favor the IF pathway.

Table 1. Rate constants corresponding to conformational isomerization of ***M*–1**, CCl_4⊂***M*–1**, CBr_4⊂***M*–1**, as well as CCl_4 in/out guest exchange at –95 °C in CD_2Cl_2; for additional experimental details, see SI.

k_n (s^{-1})	***M*–1**^{computed}	***M*–1**	CCl_4⊂***M*–1**	CBr_4⊂***M*–1**
k_{ex}	2.7	14.8±0.4	6.0±0.2	6.4±0.2
k_3 or k_4	2.6	6.8±0.3	4.6±0.2	4.6±0.2
k_{-3} or k_{-4}	0.1	8.0±0.3	1.4±0.1	1.8±0.1
k_1 ($M^{-1}s^{-1}$)	–	–	7630±290	–
k_2 ($M^{-1}s^{-1}$)	–	–	10120±220	–
k_{-1}	–	–	409±15	–
k_{-2}	–	–	161±15	–

Results and Discussion

Proton nuclei from twisted capsule changed their chemical/magnetic environments as conformer ***M*–1**(+) turned into ***M*–1**(–), and vice versa (K_3, Figure 2C). We monitored the exchange of well-separated H_A resonances from ***M*–1**(+)/***M*–1**(–) by running a series of ^{1}H EXSY measurements with different mixing times (τ_m = 0.1–2 s, Figure 3A).[21] The change in the intensity of EXSY cross and diagonal signals as a function of mixing time fit well to Bloch-McConnell equations to give rate constants k_3 and k_{-3} characterizing the conformational dynamics of ***M*–1** lacking CX_4 guests (Table 1, $k_{ex}(3) = k_3 + k_{-3}$; Figure 3D). Next, we studied the exchange of ***M*–1** diastereomers in the presence of CX_4 (X=Cl, Br). First, we probed host-guest binding dynamics by completing ^{1}H NMR titrations at –95 °C, where ***M*–1**(+) and ***M*–1**(–) are exchanging slow on the NMR time scale. Spectral changes taking place with the addition of CCl_4 to ***M*–1** are shown in Figure 3B. Specifically, a steady movement of ^{1}H NMR resonances, caused by the incremental addition of CCl_4, are consistent with the guest binding fast on the chemical shift time scale. On the other hand, the emergence of two new sets of ^{1}H NMR resonances during the titration of ***M*–1** with CBr_4 (Figure 3C),[16] corresponding to CBr_4⊂***M*–1**(+) and CBr_4⊂***M*–1**(–), revealed that all the binding processes are in the slow exchange regime. Subsequently, we measured $k_{ex}(4)$ ($k_{ex}(4) = k_4 + k_{-4}$, Figure 3D) corresponding to CCl_4⊂***M*–1**(+) exchanging with CCl_4⊂***M*–1**(–). After ***M*–1** was saturated with 390 molar

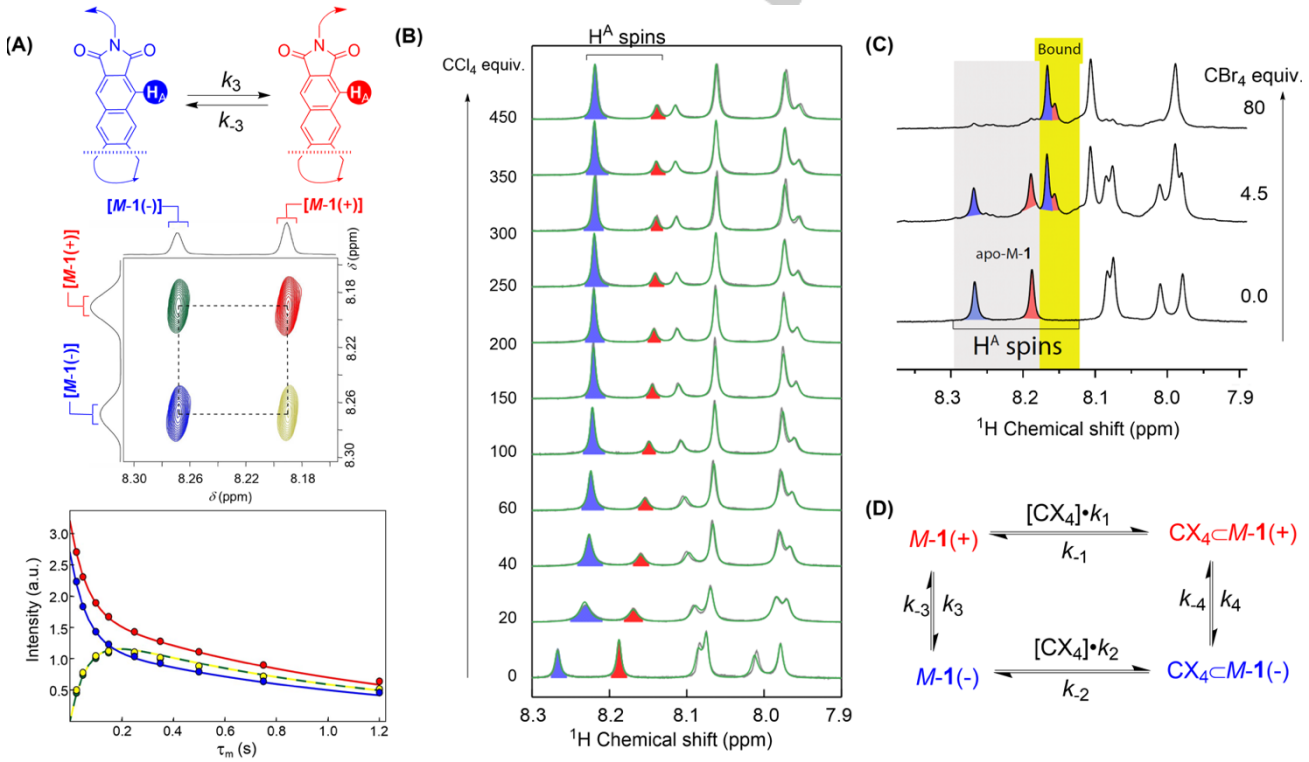

Figure 3. (A) A segment from ^{1}H EXSY spectrum (τ_m = 150 ms; –95 °C) of ***M*–1** in CD_2Cl_2 showing magnetization transfers between H_A in ***M*–1**(+) (red) and H_A in ***M*–1**(–) (blue). Exchange rate constants k_3 and k_{-3} were obtained by fitting EXSY build-up data using Bloch-McConnell matrix for two-state exchange (see ESI for details). (B) A segment from ^{1}H NMR titration of 1.5 mM ***M*–1** (CD_2Cl_2, –95 °C) with CCl_4 showing that addition of the guest caused steady changes in chemical shifts and the intensities of the peaks corresponding to H_A protons. From line-shape analysis, we obtained simulated spectra that are shown in brown. (C) A segment from ^{1}H NMR titration of 0.5 mM ***M*–1** (CD_2Cl_2, –95 °C) with CBr_4 showing the emergence of new pair of signals corresponding to the hosts holding CBr_4. (D) A scheme with rate coefficients for elementary steps in our four-state system under a thermal equilibrium.

equivalents of CCl_4, we used ^{1}H EXSY spectroscopy to complete the build-up measurements and obtain k_{ex}(4) (Table 1). To probe the interconversion rate of CBr_4⊂***M***–**1**(+) and CBr_4⊂***M***–**1**(–) (k_{ex}(4), Figure 3D), we used ^{13}C EXSY spectroscopy experiments as the proton resonances were insufficiently separated for ^{1}H EXSY spectroscopic analysis. In brief, the exchange of carbon singlets from $^{13}CBr_4$ occupying ***M***–**1**(+) and ***M***–**1**(–) gave ^{13}C EXSY buildup data (Figure S5) from which we derived rate constants k_4 and k_{-4} (Table 1). Evidently, with CBr_4 but also CCl_4 residing in the cavity of ***M***–**1**, the rate of conformational interconversion was reduced with respect to solvated ***M***–**1** (Table 1). Did the rate decrease come about via stabilization of ground CX_4⊂***M***–**1**(+) and CX_4⊂***M***–**1**(–) states, destabilization of the rate limiting transition state or both? the case for the reverse reactions, k_{-4} vs. k_{-3}. On the basis of the computed conformational interconversion (Figure 4) in which the capsule moves its methylene groups at top, we deduced that the ground state stabilization of CX_4⊂***M***–**1**(–) must be affecting k_{-4} to restrict the capsule's conformational dynamics. That is to say, if we assume that the computed mechanism of interconversion of ***M***–**1** holds for CX_4⊂***M***–**1**(–)/CX_4⊂***M***–**1**(+), then three directional C–Cl/Br···H–C hydrogen bonds should, due to a loss of directionality,[17] weaken in all but the CX_4⊂***M***–**1**(–) ground state (Figure 4).

As stated earlier, ^{1}H NMR spectrum of ***M***–**1** containing $^{13}CBr_4$ would at –95 °C show four sets of resonances corresponding to ***M***–**1**(+), ***M***–**1**(–), $^{13}CBr_4$⊂***M***–**1**(+) and $^{13}CBr_4$⊂***M***–**1**(–) (Figure 5A). The four species are in a thermal

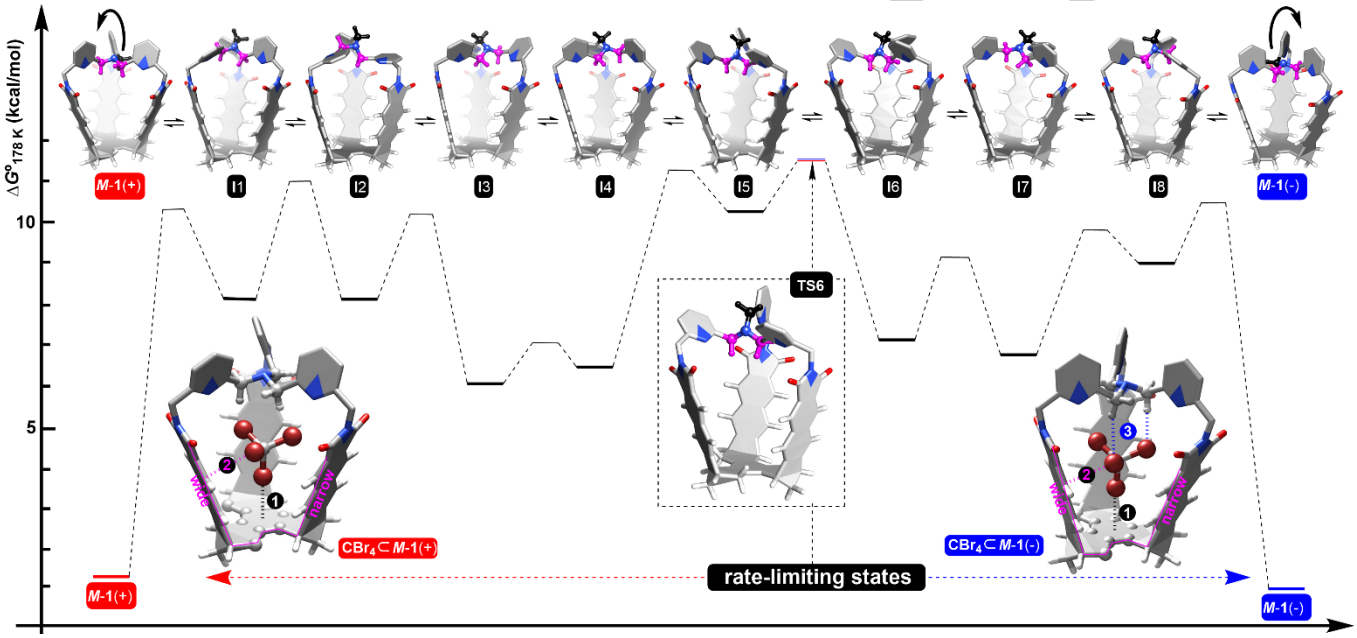

Figure 4. Schematic representation of the computed energy surface depicting the interconversion of ***M***–**1**(+) into ***M***–**1**(–). Stationary (I1–I8, ***M***–**1**(+)/(–)) and saddle points (TS1–TS9) were minimized using at the B3LYP/6-31+G* level; see SI for a movie showing the correlated motion of methylene units. Energy-minimized structures of CBr_4⊂***M***–**1**(+) and CBr_4⊂***M***–**1**(–) are shown at the bottom.

To answer the question, we used NEB and DFT methodology to generate interconversion pathways. Intermediates and transition states were further re-optimized with DFT methodology to map the potential energy surface of the transformation (Figure 4). The conversion of ***M***–**1**(+) into ***M***–**1**(–) encompassed eight high-energy intermediates, I1-I8, with TS6 (Figure 4) being the rate limiting state. In particular, chiral ***M***–**1**(+) transforms into ***M***–**1**(–) via correlated motion of TPA methylenes.[6c] As one of the methylene groups (black, Figure 4) undergoes vertical and counterclockwise swing to "flip" its axial/equatorial hydrogens, the remaining two methylenes (magenta, Figure 4) move horizontally with their hydrogens exchanging the position with respect to the bowl. Importantly, the movement of CH_2 groups is coupled with the twisting motion of the pyridine rings (see the video file in ESI). The computed activation energy $\Delta G_{ex}^{\ddagger}$ for the interconversion amounts to 9.9 kcal/mol at 178 K and is close to the experimentally determined $\Delta G_{ex}^{\ddagger}$ = 9.3 kcal/mol, thus validating the theoretical method used in this work. Importantly, the experimental k_4 for the conversion of CX_4⊂***M***–**1**(+) into CX_4⊂***M***–**1**(–) (X = Cl and Br, Table 1) was close to k_3 corresponding to ***M***–**1**(+) turning into ***M***–**1**(–) while this was not equilibrium[17] with the conformational interconversion of the capsules occurring at a faster rate than ingress/egress of CBr_4.[17] With the exchange of H_A spins (color coded in Figure 5A/B) between ***M***–**1** and $^{13}CBr_4$⊂***M***–**1** states, occurring at slower rates, we increased the mixing time ($\tau_m \geq$ 2s, Figure 5A) to allow for a detectable transfer of magnetization through in/out guest exchange processes. The appearance of a cross peak between H_A protons from ***M***–**1**(+) and ***M***–**1**(–) (K_3, Figure 5A/B) is in line with the interconversion of these two conformers occurring during τ_m = 2s. Concurrently, a peak depicting the exchange between H_A spins from $^{13}CBr_4$⊂***M***–**1**(+) and $^{13}CBr_4$⊂***M***–**1**(–) was difficult to tell apart. However, from the ^{13}C EXSY spectrum of the sample (τ_m = 2.5s, Figure 5C), a well-resolved set of signals from $^{13}CBr_4$⊂***M***–**1**(+) and $^{13}CBr_4$⊂***M***–**1**(–) as well as their cross peak manifested the exchange occurring on the time scale of the experiment. Importantly, we also noted a cross signal between free $^{13}CBr_4$ and $^{13}CBr_4$⊂***M***–**1**(–) but not $^{13}CBr_4$⊂***M***–**1**(+) (Figure 5C). It follows that the flux of CBr_4 via K_2 prevails over the K_1 pathway (Figure 5B). Indeed, by inspecting ^{1}H EXSY correlations in Figure 5A, an off-diagonal exchange signal between H_A spins from $^{13}CBr_4$⊂***M***–**1**(–) and ***M***–**1**(–) is apparent,

while there is no cross peak that would imply the exchange of $^{13}CBr_4 \subset$ ***M*–1**(+) and ***M*–1**(+). With ***M*–1**(–) binding to CBr_4 at a faster rate than ***M*–1**(+) and even more rapid interconversion of ***M*–1**(+) into ***M*–1**(–), CS (K_3–to–K_2 in Figure 5B) is the dominant route by which the recognition of CBr_4 takes place under our experimental conditions. All the same, the induced fit route starting with ***M*–1**(+) binding to CBr_4 (K_1–to–K_4 in Figure 5B) occurred at a slower rate with cross peaks below the EXSY signal-to-noise threshold. Direct conversion of ***M*–1**(+) into $CBr_4 \subset$ ***M*–1**(–), depicting the orthodox IF mechanism, was too slow to be measured with the EXSY method, if happening at all.[8a]

Finally, we performed the lineshape analysis of data from ^{1}H NMR spectroscopic titration of ***M*–1** with CCl_4 (Figure 3B) to obtain the rate coefficients corresponding to CCl_4 complexing ***M*–1**(+) and ***M*–1**(–) (Table 1; see also Figure S3.1). In this regard, equilibrium constants K_1, K_2, K_3 and K_4 as well as exchange rate constants k_3, k_{-3}, k_4 and k_{-4} (Figure 3D) were set using values obtained from already described EXSY measurements (Table 1). The dissociation rate coefficients k_{-1} and k_{-2}, chemical shifts and linewidths were then fit to the observed data using a Levenberg-Marquardt nonlinear least-squares algorithm (see ESI). In this way, the combined EXSY/lineshape analysis approach allowed us to obtain rate coefficients corresponding to all the elementary steps from thermodynamic cycle in Figure 6A. This set the stage for the flux-based analysis[8a] in which we calculated the net flux through each of the two competing pathways (F_{IF} and F_{CS}, Figure 6A) for a broad range of experimental conditions (Figure 6B); note that the fractional flux α_{CS} in Figure 6B depicts the fraction of CS route as a function of total concentration of CCl_4. Under our experimental conditions, $[CCl_4]_0$ = 0–675 mM and $[$***M*–1**$]_0$ = 1.5 mM (Figure 3B), the fractional flux through CS pathway (α_{CS}) changed from 1 to 0.2 to reveal both pathways participating in the process (Figure 6B). At critical guest concentration of $[CCl_4]_0$ = 80 mM (the function's inflection point in Figure 6B), the fractional flux is 0.5 with IF and CS occurring at equal rates (Figure 6B) so that lower concentrations of CCl_4 prefer CS

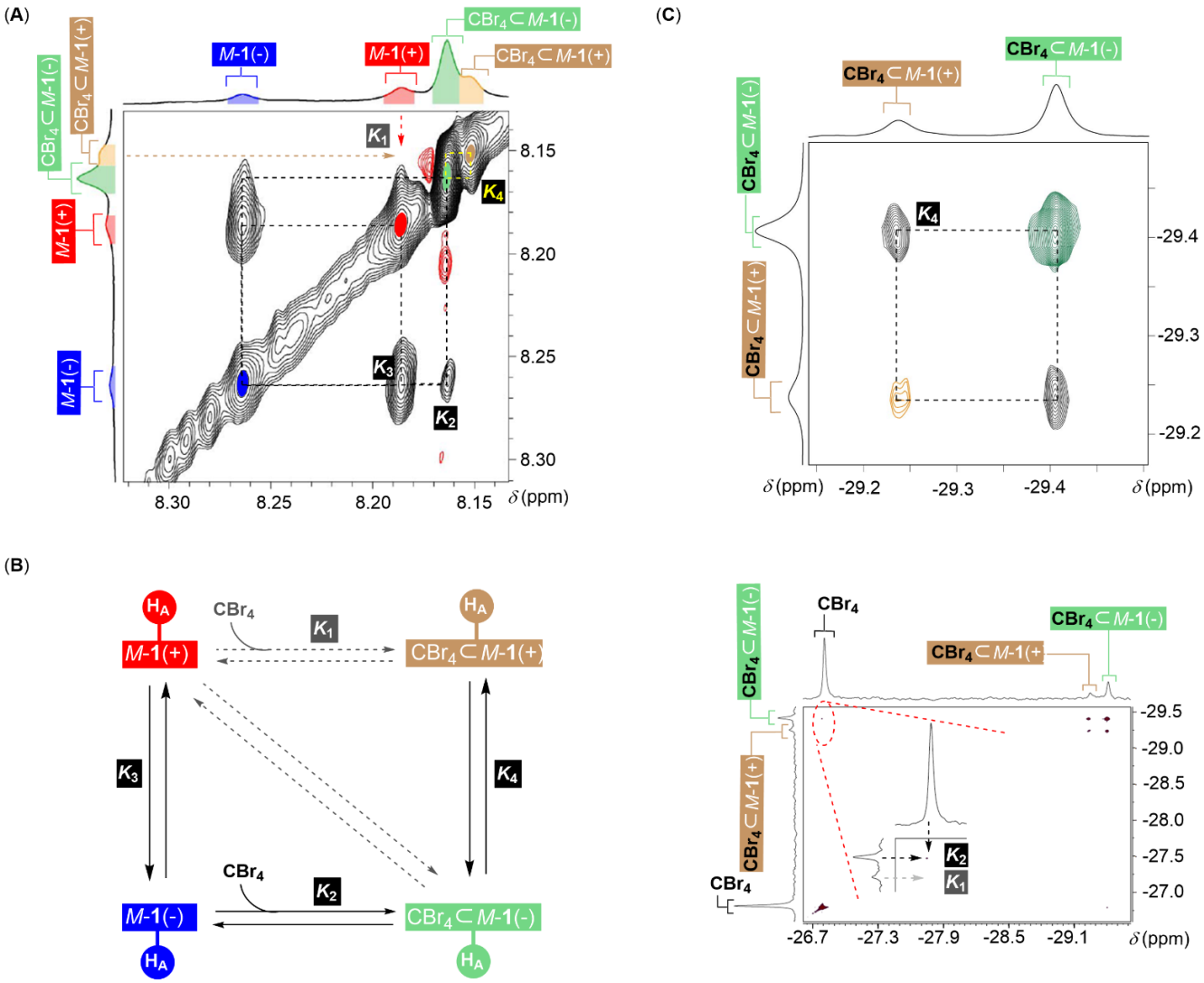

Figure 5. (A) A segment from of ^{1}H EXSY spectrum (τ_m = 2 s; –95 ºC) of 1.3 mM solution of ***M*–1** in CD_2Cl_2 containing 7.8 mM $^{13}CBr_4$ depicting the exchange of H_A spins between four states ***M*–1**(+) (red), ***M*–1**(–) (blue), $^{13}CBr_4 \subset$ ***M*–1**(+) (brown) and $^{13}CBr_4 \subset$ ***M*–1**(–) (green); note that the peaks with red contours are the artifacts. (B) A schematic depiction of the four-state exchange comprising K_1–K_4 equilibria. (C) ^{13}C EXSY spectra (τ_m = 2.5 s; –95 ºC) of 1.3 mM solution of ***M*–1** in CD_2Cl_2 containing 7.8 mM $^{13}CBr_4$ showing the spin exchange between free $^{13}CBr_4$ (black), $^{13}CBr_4 \subset$ ***M*–1**(+) (brown) and $^{13}CBr_4 \subset$ ***M*–1**(–) (green).

(α_{CS}>0.5) while higher concentrations favor the IF route (α_{CS}<0.5). By increasing the concentration of the host (1 – 10000 mM, Figure 6C) the critical guest concentration shifts to higher values while the CS still dominates at lower concentrations of CCl_4. Evidently, CS and IF are not mutually exclusive as both mechanistic pathways may take place for a range of host/guest concentrations.[8a]

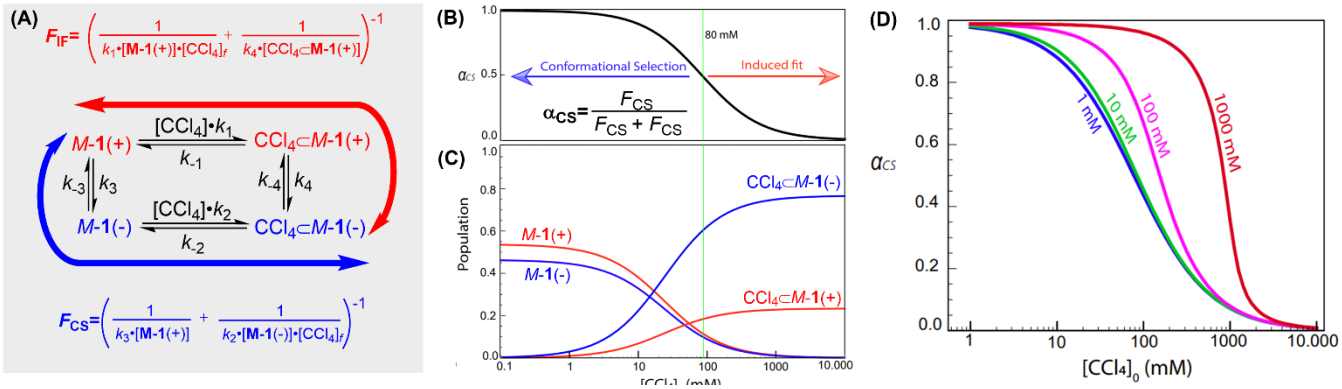

Figure 6. (A) CS (blue) and IF (red) pathways with equations describing the net flux through each. (B) Fractional flux through CS is plotted against total guest concentration ($[CCl_4]_0$ = 10^{-1} – 10^4 mM) for [***M***–**1**] = 1.5 mM. (C) Distribution of the four species in a thermal equilibrium as a function of guest concentration $[CCl_4]_0$ = 10^{-1} – 10^4 mM calculated for [***M***–**1**]$_0$ = 1.5 mM. (D) Fractional flux through the CS route (α_{CS}) calculated for [***M***–**1**]$_0$ = 1, 10, 100 and 1000 mM is plotted as a function of $[CCl_4]_0$.

Conclusion

In conclusion, the relative involvement of conformational selection (CS) and induced fit (IF) pathways by which abiotic hosts encapsulate guests can be determined with dynamic NMR spectroscopy and flux analysis.[8a] In the case of capsule ***M***–**1** trapping CCl_4, we used data from 2D EXSY and 1D NMR spectroscopic measurements to extract all of the kinetic parameters characterizing the system's dynamics; the same experimental procedure is more challenging to apply in studying complex biological systems. By means of flux-based analysis, we found that CS and IF are not mutually exclusive and occur concurrently. While the former dominates at lower guest concentrations, the latter is favored at higher concentrations. Moreover, EXSY spectroscopy is a rapid way for directly visualizing the route by which abiotic hosts capture their guests in situations where the conformational exchange and the guest binding events are all slow on the chemical shift time scale. Indeed, it should be kept in mind that such analysis provides mechanistic clarification under selected working conditions (i.e. host and guest concentrations).

To the best of our knowledge, this study is the first full description of an abiotic host undergoing competing conformational transitions and guest encapsulations. Expanding the methodology to other hosts will advance our fundamental understanding of the way by which artificial systems capture their guests. The knowledge will help designing and regulating allosteric molecular machines[22] (sequesters, catalysts, etc.) akin to those in nature[23] and for which the order by which chemical events take place is important.[24]

Acknowledgements

This work was financially supported with funds obtained from the National Science Foundation under CHE-2002781 (J.D.B.). We are grateful for the postdoctoral fellowship (to M. G.) received from the Scientific and Technological Research Council of Turkey (TUBITAK). We thank the Ohio Supercomputer Center for generous allocations of computational resources. This study made use of the Campus Chemical Instrument Center NMR facility at the Ohio State University.

Keywords: keyword 1 • keyword 2 • keyword 3 • keyword 4 • keyword 5

References

[1] Q. Cui, M. Karplus, *Protein Sci.* **2008**, *17*, 1295.
[2] (a) S. Lu, Q. Shen, J. Zhang, *Acc. Chem. Res.* **2019**, *52*, 492; (b) C. A. Hunter, H. L. Anderson, *Angew. Chem., Int. Ed.* **2009**, *48*, 7488.
[3] J.-P. Changeux, S. Edelstein, *F1000 Biol Rep* **2011**, *3*, 19.
[4] D. E. Koshland, Jr., G. Nemethy, D. Filmer, *Biochemistry* **1966**, *5*, 365.
[5] J. Monod, J. Wyman, J. P. Changeux, *J. Mol. Biol.* **1965**, *12*, 88.
[6] (a) T. Sawada, H. Hisada, M. Fujita, *J. Am. Chem. Soc.* **2014**, *136*, 4449; (b) O. Taratula, P. A. Hill, N. S. Khan, P. J. Carroll, I. J. Dmochowski, *Nat. Commun.* **2010**, *1*, 1; (c) L. Zhiquan, H. Xie, S. E. Border, J. Gallucci, R. Z. Pavlovic, J. D. Badjic, *J. Am. Chem. Soc.* **2018**, *140*, 11091; (d) A. Brugnara, L. Fusaro, M. Luhmer, T. Prange, B. Colasson, O. Reinaud, *Org. Biomol. Chem.* **2014**, *12*, 2754; (e) J. Hostas, D. Sigwalt, M. Sekutor, H. Ajani, M. Dubecky, J. Rezac, P. Y. Zavalij, L. Cao, C. Wohlschlager, K. Mlinaric-Majerski, L. Isaacs, R. Glaser, P. Hobza, *Chem. Eur. J.* **2016**, *22*, 17226.
[7] P. Csermely, R. Palotai, R. Nussinov, *Trends Biochem. Sci.* **2010**, *35*, 539.
[8] (a) G. G. Hammes, Y.-C. Chang, T. G. Oas, *Proc. Natl. Acad. Sci. U. S. A.* **2009**, *106*, 13737; (b) G. Vauquelin, D. Maes, D. C. Swinney, *Trends Pharmacol. Sci.* **2020**, *41*, 923.
[9] (a) S. Chen, M. Yamasaki, S. Polen, J. Gallucci, C. M. Hadad, J. D. Badjic, *J. Am. Chem. Soc.* **2015**, *137*, 12276; (b) W. Wang, H. Wang, L. Zhiquan, H. Xie, H. Cui, J. D. Badjic, *Chem. Sci.* **2019**, *10*, 5678; (c) J. J. Henkelis, A. K. Blackburn, E. J. Dale, N. A. Vermeulen, M. S. Nassar, J. F. Stoddart, *J. Am. Chem. Soc.* **2015**, *137*, 13252; (d) E. G. Sheetz, B. Qiao, M. Pink, A. H. Flood, *J. Am. Chem. Soc.* **2018**, *140*, 7773; (e) M. Zhang, D. Sigwalt, L. Isaacs, *Chem. Commun.* **2015**, *51*, 14620.
[10] Y. Sakata, M. Tamiya, M. Okada, S. Akine, *J. Am. Chem. Soc.* **2019**, *141*, 15597.
[11] C. M. Hong, D. M. Kaphan, R. G. Bergman, K. N. Raymond, F. D. Toste, *J. Am. Chem. Soc.* **2017**, *139*, 8013.

[12] L.-P. Yang, L. Zhang, M. Quan, Y.-L. Ma, H. Zhou, W. Jiang, S. Ward Jas, K. Rissanen, *Nat Commun* **2020**, *11*, 2740.
[13] Y.-Y. Zhan, T. Kojima, T. Nakamura, T. Takahashi, S. Takahashi, S. Hiraoka, T. Nakamura, Y. Haketa, H. Maeda, Y. Shoji, T. Fukushima, *Nat Commun* **2018**, *9*, 4530.
[14] W. Wang, T. J. Finnegan, Z. Lei, X. Zhu, C. E. Moore, K. Shi, J. D. Badjic, *Chem. Commun.* **2020**, *56*, 1271.
[15] R. Z. Pavlovic, S. E. Border, Y. Li, X. Li, J. D. Badjic, *Chem. Commun.* **2020**, *56*, 2987.
[16] J. Czescik, Y. Lyu, S. Neuberg, P. Scrimin, F. Mancin, *J. Am. Chem. Soc.* **2020**, *142*, 6837.
[17] R. Z. Pavlovic, Z. Lei, M. Gueney, R. F. Lalisse, R. G. Hopf, J. Gallucci, C. Moore, H. Xie, C. M. Hadad, J. D. Badjic, *Chem. - Eur. J.* **2019**, *25*, 13124.
[18] (a) M. Marusic, J. Schlagnitweit, K. Petzold, *ChemBioChem* **2019**, *20*, 2685; (b) C. L. Perrin, T. J. Dwyer, *Chem. Rev.* **1990**, *90*, 935.
[19] (a) T. J. Dwyer, J. E. Norman, P. G. Jasien, *J. Chem. Educ.* **1998**, *75*, 1635; (b) A. D. Bain, *Prog. Nucl. Magn. Reson. Spectrosc.* **2003**, *43*, 63; (c) Z. Zolnai, N. Juranic, D. Vikic-Topic, S. Macura, *J. Chem. Inf. Comput. Sci.* **2000**, *40*, 611.
[20] G. Henkelman, G. Johannesson, H. Jonsson, *Prog. Theor. Chem. Phys.* **2000**, *5*, 269.
[21] G. Palmer Arthur, 3rd, H. Koss, *Methods Enzymol* **2019**, *615*, 177.
[22] L. Zhang, V. Marcos, D. A. Leigh, *Proc. Natl. Acad. Sci. U. S. A.* **2018**, *115*, 9397.
[23] K. G. Daniels, N. K. Tonthat, D. R. McClure, Y.-C. Chang, X. Liu, M. A. Schumacher, C. A. Fierke, S. C. Schmidler, T. G. Oas, *J. Am. Chem. Soc.* **2014**, *136*, 822.
[24] A. Sabatino, E. Penocchio, G. Ragazzon, A. Credi, D. Frezzato, *Angew. Chem., Int. Ed.* **2019**, *58*, 14341.

Entry for the Table of Contents

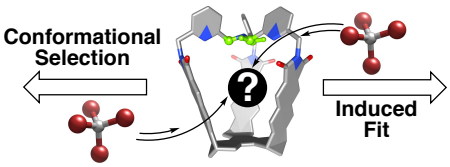

For capturing guests, abiotic hosts are found to use both conformational selection and induced-fit mechanisms. In this regard, one can easily direct the order by which encapsulation takes place for, perhaps, tuning the action of allosteric molecular machines and increasing their operational efficiency.

Institute and/or researcher Twitter usernames: